Int. J. Heat Mass Transfer. Vol. 36, No. 4, pp. 875–886, 1993
Printed in Great Britain

0017–9310/93 $6.00 + 0.00

Interacting, convecting, vaporizing fuel droplets with variable properties

C. H. CHIANG and W. A. SIRIGNANO
Department of Mechanical and Aerospace Engineering, University of California, Irvine, CA 92717, U.S.A.

(*Received* 10 *January* 1992 *and in final form* 22 *May* 1992)

Abstract—Two vaporizing droplets moving in tandem are numerically investigated. The forced convection of the gas phase, the transient deceleration due to the drag force, the surface regression, the relative motion between the two droplets, the internal circulation, transient heating of the liquid phase, and variable properties are considered. The unsteady, axisymmetric description of the global flowfield, the behavior of the interacting droplets, and the transient variation of the droplet spacing are presented. The dependencies on initial droplet Reynolds number, initial droplet spacing, initial droplet size ratio, variable properties, transfer number are determined. The critical droplet size ratio dividing the region where droplets collide from the region where they separate is determined. Correlations for the drag coefficients, Nusselt and Sherwood numbers of the lead droplet and the downstream droplet are obtained.

INTRODUCTION

THE COMPLEX combustion processes occurring in liquid-fueled combustors with direct spray injection are basically heterogeneous in nature, involving vaporization and combustion of a cloud of droplets that interact with a gaseous environment and also with each other. In the dense-spray regions near the fuel nozzle, various coupled processes may occur, including atomization, droplet collision, coalescence, breakup, and interphase transport processes. As a result spray droplets can behave quite differently to isolated droplets. A very comprehensive analysis that takes into account the details around the interacting droplets is required to provide the fundamental information for the overall spray calculation.

There has been recent interest in the study of interactions between droplets. The solid–particle interactions due to hydrodynamic as well as non-hydrodynamic forces in the low Reynolds number flow were examined by Happel and Brenner [1], Batchelor and Green [2], Jeffrey and Onishi [3], etc. Tal and Sirignano [4] and Tal *et al.* [5] studied the heat and mass transfer in an array of non-vaporizing particles with forced convection at Reynolds number $\sim O(100)$. These studies indicate the importance of hydrodynamic as well as thermal interactions between solid spheres.

Most of the existing work on vaporizing droplet interactions has been primarily concentrated on droplets in artificial arrays with low flux conditions and in the absence of forced convection, internal circulation and transient heating, and thus are simply diffusion analyses [6–10]. Law and colleagues [11] have shown that the existing diffusion-dominating theory overpredicts the intensity and persistence of interaction. They also observed that even the interactive buoyant convection can substantially augment the interaction effects. A detailed review of droplet array theory is provided by Sirignano [12].

The full consideration of forced convection of the gas phase, internal circulation and transient heating of the liquid phase, transport processes occurring at the vaporizing droplet interface requires the solution of the complete set of the Navier–Stokes equations, with energy and species equations, combined with appropriate boundary conditions.

A simple analytical approach, by assuming steady flow and constant properties, to investigate the interactions on drag coefficients and mass transfer coefficients of two adjacent spheres has been employed by Asano *et al.* [13]. The interacting effects due to geometric parameters and mass transfer are identified by their proposed correlations where the heat transfer effect is excluded.

Patnaik [14] studied numerically the interaction between two vaporizing droplets which are moving in tandem with respect to the free stream. The numerical algorithm for flow passing over a vaporizing droplet was employed (Patnaik *et al.* [15]). The downstream solution of the lead droplet is used for the inflow conditions to the solution of the downstream droplet. This research neglects the influence of the downstream droplet on the lead droplet. Most importantly, the variation of the transient droplet spacing resulting from the difference in retardation of the droplets was not taken into account.

Recently, Raju and Sirignano [16, 17] have examined in detail the same problem (two droplets moving in tandem in an intermediate Reynolds number flow) over a limited range of different initial Reynolds numbers, droplet spacings, and droplet radii ratios. The implicit finite difference method together with a grid-generation scheme developed by Thompson *et al.* [18] was used to solve the full transport equations. The results showed that the droplet interactions are evi-

NOMENCLATURE

$A_{d,i}$ non-dimensional droplet deceleration, $A'_{d,i}R'^2_{i,0}\rho'_{g,z}/\mu'_z U'_z$
B_H effective heat transfer number, $C'_{pg,film}(T'_z - T'_s)(1-(Q'_l/Q'_g))/L'_s$
C_D total drag coefficient, $C_p + C_f + C_t$
C_f friction drag coefficient, $2F'_f/(\rho'_{g,z}(U'_z - U'_{d,i})^2\pi R'^2_i)$
C_p pressure drag coefficient, $2F'_p/(\rho'_{g,z}(U'_z - U'_{d,i})^2\pi R'^2_i)$
C'_{pg} specific heat of gas
C_t thrust drag coefficient, $2F'_t/(\rho'_{g,z}(U'_z - U'_{d,i})^2\pi R'^2_i)$
D non-dimensional droplet spacing, $D'/R'_{1,0}$
$\mathscr{D}_g$ non-dimensional diffusivity of gas phase, $\mathscr{D}'_g/\mathscr{D}'_{g,z}$
F' force
L' latent heat of vaporization
Nu Nusselt number, $R_i\int_0^\pi \kappa_g(\partial T_g/\partial n)\sin\theta\,d\theta/(1-T_s)$
p' pressure
Q' heat flux
R non-dimensional instantaneous droplet radius, $R'/R'_{1,0}$
Re_g gas-phase Reynolds number, $R'_{1,0}U'_{z,0}\rho'_{g,z}/\mu'_z$
Re_m modified Reynolds number, $2R'_iU'_z\rho'_{g,z}/\mu'_{film}$
Sh Sherwood number, $R_i\int_0^\pi \rho_g\mathscr{D}_g(\partial Y_f/\partial n)\sin\theta\,d\theta/(Y_{f,z}-Y_{f,s})$
T non-dimensional temperature, T'/T'_z
U_d non-dimensional droplet velocity, $U'_d/U'_{z,0}$
U_z non-dimensional free stream velocity, $U'_z/U'_{z,0}$
V non-dimensional velocity, $V'/U'_{z,0}$
Y_f mass fraction.

Greek symbols
θ tangential direction
κ_g conductivity of gas phase, $\kappa'_g/\kappa'_{g,z}$
μ'_g viscosity of gas phase
ξ, η non-orthogonal coordinates
ρ'_g density of gas phase
ρ'_l density of liquid phase
τ_{Hg} gas hydrodynamic diffusion time, $t'\mu'_z/(R'^2_{1,0}\rho'_{g,z})$.

Subscripts
d droplet
f fuel
film film conditions, average of ambient and surface conditions
g gas phase
i numerical index for droplets, 1 = lead droplet, 2 = downstream droplet
iso isolated
l liquid phase
n normal direction
r radial direction
s at the droplet surface
t tangential direction
v volumetric average
z axial direction
0 initial conditions
θ tangential direction
∞ free stream conditions.

Superscripts
$'$ dimensional quantity
$*$ estimate at the new time step.

dent for initial Reynolds numbers of 50 to 200 and for initial droplet spacings of 2 to 15 droplet diameters. The droplets can either collide or move apart depending upon the initial conditions. There exists a critical ratio of initial droplet diameters below which droplet collision becomes unlikely. Both the studies of Patnaik *et al.* [15] and Raju and Sirignano [16, 17] consider the variable density, but other thermophysical properties are constant. The initial droplet temperature and ambient temperature are used as the reference temperature for the liquid and gas-phase property evaluation, respectively. Using the detailed analysis of a vaporizing droplet in a convective field with variable thermophysical properties by Chiang *et al.* [19], the drag coefficient can be overestimated by at least 20% if the above choice of reference is made for constant-property calculation. This magnitude of error in the two droplet calculation could change qualitative conclusions about separation or attraction of droplets over a wide range of parameters. As a result, thermal dependence of physical properties must be properly included in the high temperature spray analysis.

Our present research aims to advance the fundamental understanding of the vaporization phenomena in droplet clouds where interaction effects between vaporizing droplets in an intermediate Reynolds number flow are of interest by extending the study of Raju and Sirignano [16, 17] to include the effect of variable properties.

PHYSICAL DESCRIPTION

The configuration and numerical mesh under this study is sketched in Fig. 1 where the flow passing over two vaporizing droplets moving in tandem is shown. The flow is laminar and axisymmetric with initially uniform ambient conditions specified by U'_∞, T'_∞,

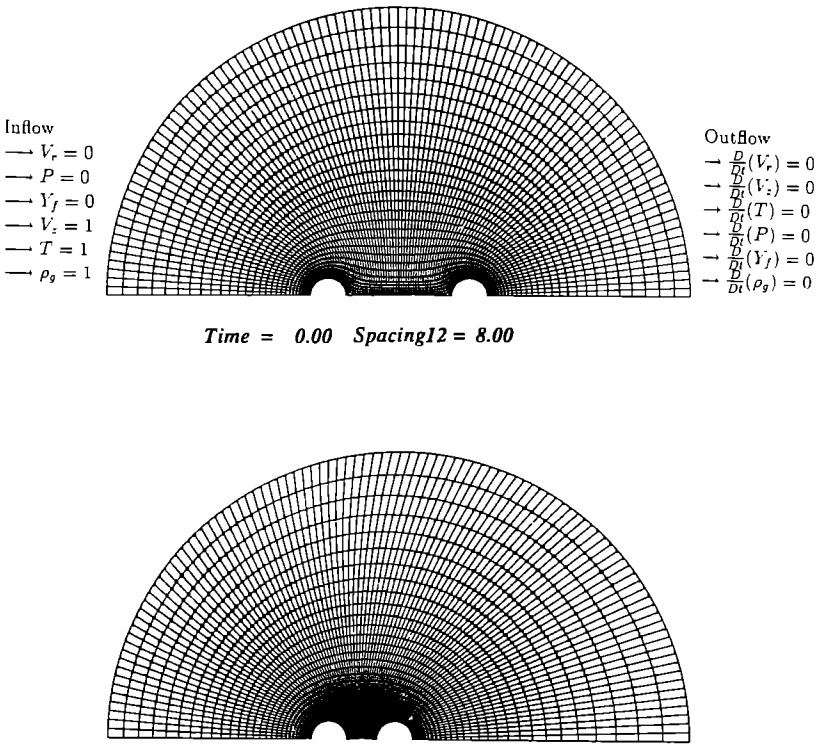

FIG. 1. Flow field configuration and grid distribution at two different times for the case of droplet collision.

$\rho'_{g,s}$, p'_s, and $Y_{f,s} = 0$. The initial droplet spacing is also prescribed. The frame of reference is fixed to the center of the lead droplet. The problem can be viewed as an impulsively started flow over a fixed droplet and a moving downstream droplet aligned in tandem. As the flow develops, the droplets experience different drag forces associated with friction, pressure, and non-uniform blowing due to evaporation. The drag force of the lead droplet decelerates the free-stream velocity in a relative sense. It is necessary to account for the movement of the second droplet toward or away from the lead droplet depending upon the relative acceleration (or deceleration) between the two droplets.

The liquid temperature is initially uniform throughout the droplet. Soon after the droplets are injected into the hot gas stream, the droplets are heated by the gas. The composition of the gas mixture is changed due to the presence of droplet vaporization. The cold fuel vapor which is generated by the lead droplet is convected downstream and alters the local environment of the second droplet.

SOLUTION PROCEDURE

The basic assumptions, the system of axisymmetric, unsteady equations and the corresponding numerical method for each equation are the same as for the single droplet case. The details are given in Chiang *et al.* [19]. It is possible to modify the single droplet code to model the multi-droplet case without a major change of the overall algorithm. All the routines for the liquid phase and interface conditions in the single droplet case are slightly modified so that they can be employed for the lead and downstream droplets. The routines for the gas-phase equations remain the same as in the single droplet case. The overall solution procedure needs two additional routines to deal with variation of spacing and grid generation, respectively.

Treatment of droplet movement

The temporal variation of spacing is determined by the change of relative droplet speed which is dependent upon the relative acceleration (or deceleration) between the two droplets.

The droplet deceleration can be expressed as

$$A_{d,i} = \frac{dU_d}{d\tau_{Hg}} = -\frac{3}{8}\frac{\rho'_\infty}{\rho'_l}\frac{(U_\infty - U_{d,i})^2}{R_i} Re_g C_D. \quad (1)$$

The change of relative velocity during a computational time step for the droplets is

$$\Delta U_{d,i} = \int_0^{\Delta\tau_{Hg}} A_{d,i}\, d\tau_{Hg}. \quad (2)$$

Since the velocity of the lead droplet remains zero in our frame of reference ($U_{d,1}(\tau_{Hg}) = 0$), it is then necessary to decelerate the whole gas velocity field by $\Delta U_{d,1}$.

$$V_{z,g}(\tau_{Hg}+\Delta\tau_{Hg}) = V^*_{z,g}(\tau_{Hg}+\Delta\tau_{Hg})+\Delta U_{d,1}.$$

The velocity of the downstream droplet is corrected as

$$U_{d,2}(\tau_{Hg}+\Delta\tau_{Hg}) = U_{d,2}(\tau_{Hg})-\Delta U_{d,2}+\Delta U_{d,1}. \quad (3)$$

The droplet spacing is then determined by

$$D(\tau_{Hg}+\Delta\tau_{Hg}) = D(\tau_{Hg})+\frac{Re_g}{2}\int_0^{\Delta\tau_{Hg}} U_{d,2}\,d\tau_{Hg}. \quad (4)$$

Since the equation solvers for the liquid phase and the interface-boundary-condition solver in the single droplet case require that the computations are performed with respect to a non-Newtonian coordinate fixed with the droplet itself, in the present study care must be taken for the computation for the downstream droplet. For instance, the change of a grid position in the z-direction during a computational step is accompanied by the change of droplet spacing as well as the droplet regression. Hence the component due to the change of spacing must be eliminated when $(\partial z/\partial\tau_{Hg})$ (the derivative of the z-coordinate with respect to time) is evaluated in liquid-phase computation for the downstream droplet. Other detailed procedures are available in Raju and Sirignano [17].

Grid generation

The generation of the computational grid requires more detailed considerations. The grid points must conform to the shapes of the droplet surfaces to avoid errors due to interpolation. A general method of generating boundary-fitted coordinate systems allows the curvilinear coordinates to be solutions of an elliptic partial differential system in the physical plane, with Dirichlet boundary conditions on all boundaries. One coordinate is specified to be constant on each of the boundaries, and a monotonic variation of the other coordinate around each boundary is specified.

In the present calculation, the TOMCAT code [18] is employed to accommodate the changing boundary shapes due to the droplet regression as well as the change of droplet spacing. The computational grid is generated from the solution of a quasi-linear elliptic system of equations with the physical coordinates $z(\xi, \eta)$ and $r(\xi, \eta)$ as the dependent variables. The source terms in the Poisson equations are used to control the grid size near the specified constant ξ_i and η_i lines and points (ξ_j, η_j).

Since the gradients of all variables are expected to be very large within the boundary layer, the first six constant η lines have been placed next to the droplet surface in order to resolve accurately the complex transport processes occurring there. Also, the rear stagnation point of the lead droplet and the front stagnation point of the downstream droplet are acting as the attracting source points to pull over the grid lines in order to obtain better resolutions in the wake region between two droplets. The quasi-linear system of Poisson equations is solved by finite-difference discretization using the successive-over-relaxation (SOR) technique.

At each new time step, the elliptic system is resolved for the transformed coordinates with the new boundaries. The grid points in the rectangular transformed plane thus remain stationary, and the effect of the movement of the coordinate system in the physical plane is just to change the values of the physical coordinate $[z, r]$ at the fixed grid points in the rectangular transformed plane. The coordinate values at the previous time step can serve as the initial guess, so that the iteration will converge rapidly. After the grid system moves, the metrics of transformation have to be updated. Since the coordinates in the physical domain at the gas/liquid interface are no longer orthogonal, the directional (normal and tangential) derivatives with respect to constant ξ or η surface in the interface-boundary-condition solver are taken from Thompson *et al.* [20].

The selection of the parameters, which is associated with the inhomogeneous terms of the Poisson equations, to control grid size is a very important task. The preliminary results from some test runs show that the numerical solutions are not very sensitive to the values of attraction amplitudes and decay factors (predicted drag coefficients, and Nusselt and Sherwood numbers are within 5% variation), but too strong an attraction amplitude may produce over-skewed grids and cause numerical instability. At first, one set of parameters is chosen to produce a grid distribution such that the grid sizes near the gas/liquid interface satisfy the CFL stability condition. The final set of attraction amplitudes and decay factors are determined when further reduction in grid size (more attraction toward interface) only results in less than 1% change in drag coefficient. The grid generation currently has 101×31 points for the gas phase and 31×30 points for the liquid phase. We have learned that the resolution within the boundary layer of both gas and liquid phase is controlled by Δr (along radial direction) only. The grid size along the azimuthal direction ($\Delta\theta$) does affect the accuracy of the integration and hence the total heat flux into the droplet.

A typical grid distribution at the beginning and at the final computational time for the case of droplet coalescence is shown in Fig. 1.

RESULTS AND DISCUSSIONS

The code has been developed successfully on the Apollo domain-3000 workstation and tested on a Convex 240 computer. The computations are performed on a CRAY Y-MP supercomputer. Depending on the input parameters, a time step ranged from 0.0005 to 0.001 is employed. A typical computation requires on average 1 s of CPU time per time step.

Since the problem involves multidimensional variables, an exhaustive numerical study of all possible combinations of parameters cannot be performed. Therefore, we have concentrated our attention on a

Table 1. Values of physical parameters used in the base case computation

Parameter	Value
Initial Reynolds number, gas phase, $=2Re_g$	100.0
Relative velocity of drop [m s^{-1}]	15.0
Free stream temperature [K]	1000.0
Combustor pressure [atm]	10.0
Prandtl number, gas phase	0.714
Prandtl number, liquid phase	14.92
Schmidt number, gas phase	3.26
Molecular weight, oxidizer [kg kmol^{-1}]	29.0
Molecular weight, fuel, *n*-decane [kg kmol^{-1}]	142.28
Droplet initial temperature [K]	300.0
Viscosity ratio, $\mu_l'/\mu_{g,s}'$	21.44
Density ratio, $\rho_l'/\rho_{g,s}'$	209.19
Specific heat at constant pressure ratio, $C_{pl,0}'/C_{pg,s}'$	1.94
Latent heat/specific heat of liquid [K]	126.28

detailed study of the interaction effects arising from the variations of initial Reynolds number, initial droplet size ratio, and ratio of initial spacing to lead droplet radius and from different transfer numbers resulting from different fuel types, ambient temperatures, and initial droplet temperatures.

Tables 1 and 2 summarize the values of physical parameters in the base case simulation and the main parameters used for different cases examined in the present work, respectively.

The results are presented in the following four subsections. The first three subsections give a description of the local, as well as overall, behaviors of the interacting droplets for the base case. Most of the results show that the behavior of the lead droplet is qualitatively in agreement with that of an isolated droplet. The general properties for the single droplet are depicted in detail in Chiang *et al.* [19]. Hence, the discussion in these three subsections is primarily concentrated on the downstream droplet. The transient variation of spacings due to different initial spacing, initial size ratio, initial Reynolds numbers, initial droplet temperature, and transfer numbers are given in the fourth subsection. Subsection five presents the correlations of the drag coefficient and Nusselt and Sherwood numbers for the lead and the downstream droplet, respectively.

Results for the global flow field

Figures 2 and 3 portray the gas-phase velocities, as well as the contour plots of mass fraction, temperature, vorticity and liquid-phase streamlines, at $\tau_{Hg} = 3$ when the spacing has been reduced from the initial value of 8 to 3.71. The spacings shown in the following figures are non-dimensionalized with respect to initial radius of the lead droplet. When the spacing equals $R_1 + R_2$, droplet collision occurs. The downstream droplet is partially covered by the recirculation zone behind the leading droplet. As a result, the velocities approaching the downstream droplet are much less than and sometimes opposite to the velocities upstream of the lead droplet. Hence, a small relative

Table 2. Main parameters considered in each case of the two-droplet study

Case[a]	Re_g	R_2'/R_1'	$D'/(R_{1,0}')$	Case	Re_g	R_2'/R_1'	$D'/(R_{1,0}')$
1	100	1	8	21	100	0.575	4
2	100	1	12	22	100	0.585	4
3	100	1	16	23	100	0.605	4
4	100	1	4	24	100	0.620	4
5	10	1	8	25	100	0.640	4
6	25	1	8	26	100	0.7	4
7	50	1	8	27	50	0.7	4
8	125	1	8	28	50	0.5	4
9	100	0.2	8	29	30	0.732	8
10	100	0.4	8	30	50	0.732	8
11	100	0.725	8	31	50	0.770	8
12	100	0.732	8	32	50	0.785	8
13	100	0.740	8	33	50	0.800	8
14	100	0.748	8	34[b]	100	1	8
15	100	0.755	8	35[c]	100	1	8
16	100	0.770	8	36[d]	100	1	8
17	100	1.5	8	37[e]	100	1	8
18	100	2.0	8	38[f]	100	1	8
19	100	0.5	4	39[g]	100	1	8
20	100	0.550	4	40[h]	100	1	8

[a] Initial ambient temperature = 1000 K, droplet temperature = 300 K, fuel = *n*-decane, variable property and axisymmetric calculation for all cases except cases indicated by the footnotes.
[b] Constant-property calculation, $T_{ref} = T_{\infty}$.
[c] Initial ambient temperature = 800 K.
[d] Initial ambient temperature = 1250 K.
[e] Initial ambient temperature = 1500 K.
[f] Initial droplet temperature = 400 K.
[g] Fuel: *n*-hexane.
[h] Fuel: *n*-octane.

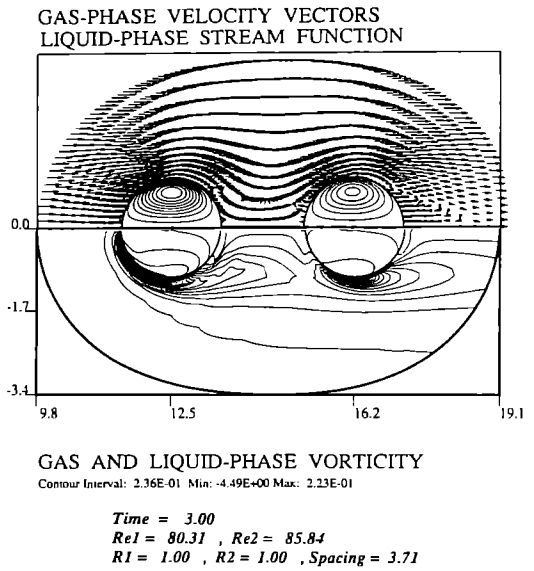

FIG. 2. Instantaneous gas-phase velocity vectors, vorticity contour, and liquid-phase streamfunction at time = 3.

Reynolds number flow passes over the downstream droplet and introduces only a small recirculation zone. The strength of the liquid-phase stream function for the downstream droplet is only half of the strength for the lead droplet. It may be primarily attributed to the considerably lower shear stress acting upon the downstream droplet.

The lower part of Fig. 2 illustrates the diffusion and convection associated with the gas-phase vorticity at the gas/liquid interface. A high gradient of vorticity occurs at the front region of the lead droplet while a smaller gradient of vorticity appears at the side of the downstream droplet. The smaller magnitude and more symmetric variation for the liquid-phase vorticity occur with the downstream droplet.

In Fig. 3, the thermal boundary layer structure of the downstream droplet is significantly different from that of the lead droplet (in terms of thickness and distribution). The liquid-phase isotherms indicate that the internal circulation develops faster for the lead droplet. For the downstream droplet, the conduction heating is the dominating heat transfer mechanism.

The mass fraction contours show a high concentration gradient near the lead droplet and a low concentration gradient at the downstream droplet. The fuel vapor generated by the lead droplet is convected downstream and alters the mixture composition of the surrounding environment near the downstream droplet. The relatively rich fuel mixture is usually cold enough to change the surrounding thermal environment of the downstream droplet significantly. Hence, the heat and mass transfer rates for the downstream droplet are reduced due to the presence of fuel vapor.

Local properties along the droplet surface

As the downstream droplet approaches the near wake region of the lead droplet, it experiences less convection and a smaller magnitude of vorticity. Figure 4 indicates that the position for the maximum surface vorticity of the downstream droplet at $\tau_{Hg} = 3$ moves to the $\theta = 90$ plane. Also, the surface vorticity at the rear portion is positive, since no flow separation occurs there. The downstream droplet is covered by the wake of the lead droplet and is in a very low Reynolds number flow field which makes separation impossible. The negative shear stress at the front stag-

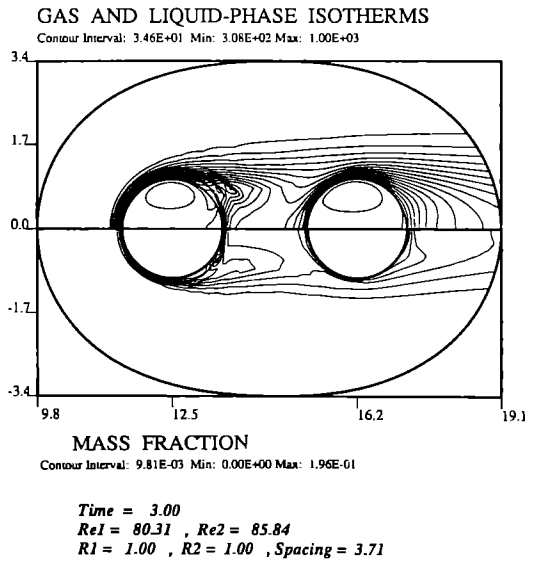

FIG. 3. Temperature and mass fraction contour plot at time = 3.

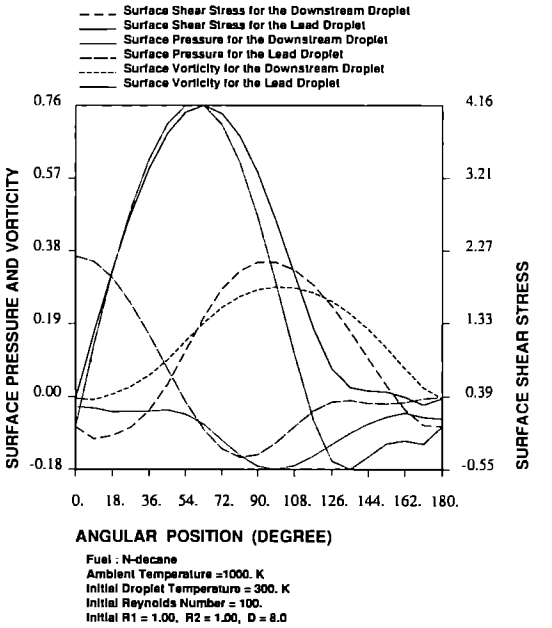

FIG. 4. Surface shear stress and pressure distribution time = 3 for the lead droplet and the downstream droplet.

nation region of the downstream droplet is caused by the recirculating flow behind the lead droplet.

Due to the action of the recirculating wake, the pressure at the stagnation point of the downstream droplet only slightly recovers from the pressure at the rear stagnation point of the lead droplet as demonstrated in the same Fig. 4. As the spacing decreases, less recovery occurs. The pressure drag of the downstream droplet becomes smaller when compared to that of the lead droplet as the droplets approach each other.

Figure 5 compares the local Nusselt and Sherwood number variations at the droplet surfaces. The decrease of the Nusselt number with time at the rear part of the lead droplet and at the front stagnation region of the downstream droplet are caused by the approach of the downstream droplet. As the spacing is reduced, the increase of cold mixture density, combined with the decrease in velocities at the wake region, serve to retard the heat exchange. The increase of Nusselt number at the rear part of the downstream droplet is caused by the hot ambient stream entrained by the recirculating flow. A similar trend can be observed for the local Sherwood number. As the same figure shows, the highly non-uniform distribution of the surface temperature for the downstream droplet is due to the slow liquid circulation which cannot distribute energy efficiently in the streamwise direction. As a result, the distribution of surface temperature is similar to that of the local Nusselt number. The heat flux is diffused primarily in the radial direction within the downstream droplet. The slow thermal mixing usually causes a small cold region at the front and a large hot region at the rear of the downstream droplet.

Overall behaviors of the two droplets

In this subsection, the drag coefficient, and Nusselt and Sherwood numbers for the lead droplet and the downstream droplet for the case of approaching droplets are presented. The results for an isolated droplet in the same convective flow field are also presented for comparison. Figure 6 shows that the drag coefficient of the lead droplet drops about 6% from its isolated-droplet value due to the interaction with the downstream droplet. The discrepancy increases as the droplet spacing decreases (note that the time goes in the direction of reduction in Reynolds numbers). The downstream droplet experiences noticeably lower drag because of the wake effect. Our numerical result confirms the experimental study of Temkin and Ecker [21] which indicated that the second droplet can experience reductions in the drag coefficients as high as 50% relative to its independent drag.

Previous research [19] has indicated that the constant-property calculation may overestimate the drag coefficient by as much as 20% of the variable property calculation if the properties are constant at the far-stream value. Figure 6 shows that the individual drag coefficients of both droplets are overpredicted in the constant-property calculation. Since the property gradients in the flowfield of the downstream droplet are smaller than those of the lead droplet, the overestimation is larger for the lead droplet than for the downstream droplet.

The breakdown of the total drag coefficient into three components is shown in Fig. 7. The difference in friction drag generally contributes most of the drag difference between the lead droplet and the isolated droplet. Both pressure and friction drag coefficients of the downstream droplet are much lower than those of the lead droplet. The sharp drop of the total drag

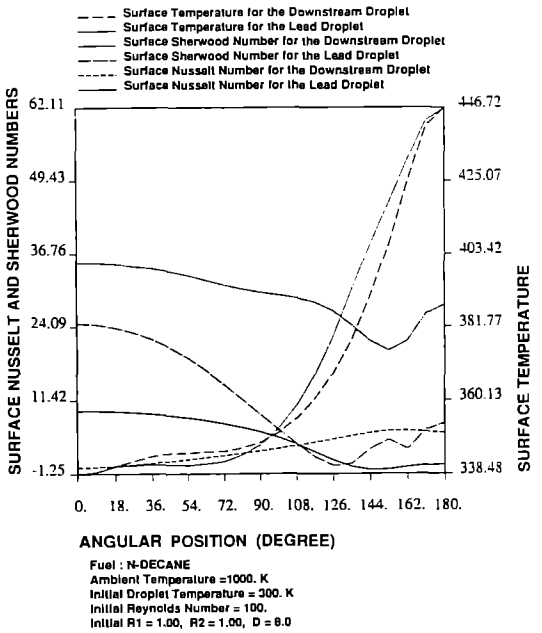

FIG. 5. Surface Nusselt and Sherwood numbers, and temperature distribution at time = 3 for the lead droplet and the downstream droplet.

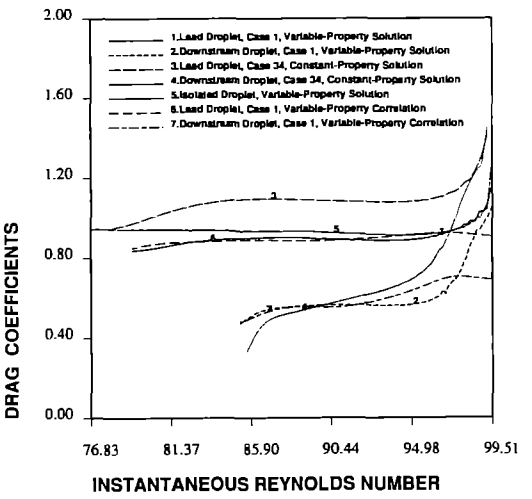

FIG. 6. Time variation of drag coefficients and correlations for the lead droplet and the downstream droplet.

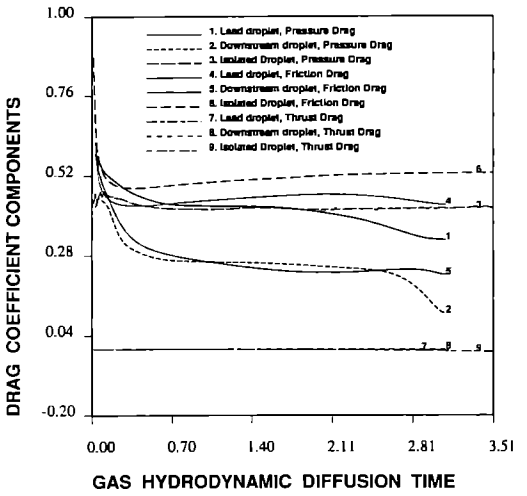

FIG. 7. Time variation of the three drag components for the lead droplet and the downstream droplet.

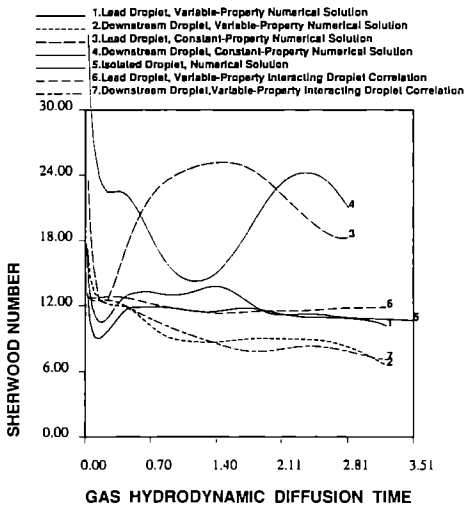

FIG. 9. Time variation of average Sherwood numbers and correlations for the lead droplet and the downstream droplet.

at the time when the two drops are about to collide is mainly attributed to the reduction in pressure drag.

Figures 8 and 9 present the overall Nusselt and Sherwood numbers, respectively. The difference in Nusselt number between two droplets indicate that wake effects tend to reduce significantly the heat transport to the downstream drop. For the lead droplet, the influence of the downstream droplet is not negligible even when the spacing is about four droplet diameters. Other results for the cases of separating drops show that the Nusselt numbers for the lead and downstream droplets behave as for the isolated droplet during the final period of calculation. The Sherwood number of the downstream droplet indicates a longer relaxation period for the mass exchange process, which is caused by the upstream droplet, throughout our calculation. Generally, the constant-property solutions overestimate the Nusselt and Sherwood numbers, the variable property solutions for either of the two droplets falls below the isolated droplet value, and the value for the lead droplet exceeds the value for the downstream droplet.

Note that the current definitions of Nusselt and Sherwood numbers are

$$Nu = \frac{R_i \int_0^{\pi} \kappa_g \frac{\partial T_g}{\partial n} \sin\theta \, d\theta}{1 - T_{ave,s}}$$

and

$$Sh = \frac{R_i \int_0^{\pi} \rho_g \mathscr{D}_g \frac{\partial Y_f}{\partial n} \sin\theta \, d\theta}{Y_{f,\infty} - Y_{f,ave,s}}$$

which are different from those of Haywood *et al.* [22] where Nusselt and Sherwood numbers are defined as

$$Nu_2 = R_i \int_0^{\pi} \frac{\kappa_g \frac{\partial T_g}{\partial n} \sin\theta \, d\theta}{1 - T_s}$$

and

$$Sh_2 = R_i \int_0^{\pi} \frac{\rho_g \mathscr{D}_g \frac{\partial Y_f}{\partial n} \sin\theta \, d\theta}{Y_{f,\infty} - Y_{f,s}}.$$

The latter definitions of Nusselt and Sherwood numbers are dependent upon azimuthal grid size.

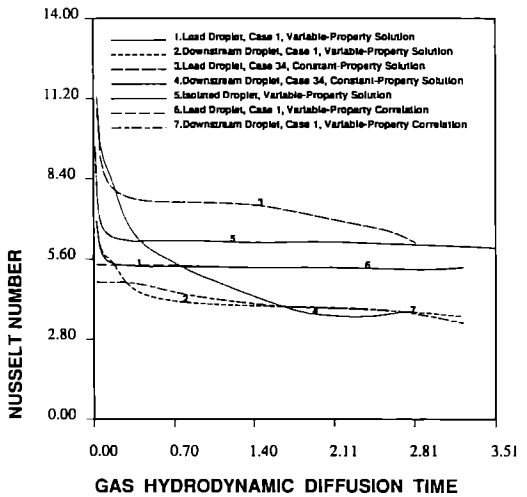

FIG. 8. Time variation of average Nusselt numbers and correlations for the lead droplet and the downstream droplet.

The transient variation of spacing

The determination of whether two droplets will collide or separate after they are suddenly introduced into a combustor is of great interest. The droplet deceleration is proportional to its drag coefficient and inversely proportional to its radius. The change of spacing is proportional to the relative deceleration between the two droplets and can be expressed as follows:

ΔD (differential change of spacing during a time step)

$$\propto (A_{d,2} - A_{d,1}) * (\Delta\tau_{Hg})^2 \propto \left(\frac{C_{D,2}}{R_2} - \frac{C_{D,1}}{R_1}\right)$$

where A_d is the droplet deceleration and $\Delta\tau_{Hg}$ is a computational time step in gas-phase hydrodynamic diffusion time scale. The subscripts 1, 2 correspond to the lead and downstream droplet, respectively. Positive ΔD will result in droplet separation while negative ΔD means that droplets collision eventually occurs. In general, $C_{D,1}$ is larger than $C_{D,2}$. If R_2 is larger than or equal to R_1, droplets will collide. On the contrary, if R_2 is much smaller than R_1, droplet separation is most likely to occur.

The transient variation of center-to-center-spacings for the cases of different initial spacing and for the case of different initial droplet size ratio is depicted in Fig. 10. The droplet collision is likely for initially equal-sized droplets, even when the droplets are initially spaced 8 diameters away. Temkin and Ecker [21] indicated that significant wake effects can still be detected by the downstream droplet even if it is located at 15 droplet diameters away.

The drag coefficients of the two droplets for initial spacing of 4, 8 and 16 are shown in Fig. 11. The smaller the initial spacing, the more the lead droplet drag coefficient deviates from its isolated value and the greater the drag coefficient is reduced for the downstream droplet. A similar trend in Nusselt number is also observed as portrayed in Fig. 12. The Nusselt number of the lead droplet does not depend upon droplet spacing when initial droplet spacing is larger than 6 diameters. However, the Nusselt number of the downstream droplet is still very sensitive to the variation of droplet spacing.

Figure 10 also demonstrates that droplet collision or separation is primarily determined by the droplet size ratio. Generally, the larger the difference in droplet sizes, the faster they approach each other (or separate away). For the case of $R_2 = 0.74$, droplet separation occurs at a very early time, but eventually droplet coalescence prevails. The results of Raju and Sirignano [17] indicate that there exists a bifurcation point depending upon the critical ratio of $R'_{2,0}/R'_{1,0}$ below which droplet coalescence becomes unlikely. The results now predict that $R_2 = 0.74$ is very close to the bifurcation point, so that the droplets spend more time under the influence of each other. A detailed investigation of the critical ratio of $R'_{2,0}/R'_{1,0}$ in determination of the relative droplet movement for the cases of initial spacing = 8 and initial spacing = 4 is displayed in Fig. 13. The droplet spacings remain nearly constant close to the critical droplet size ratio. Below this value, droplet separation is predicted. Above this value, droplet collision becomes very poss-

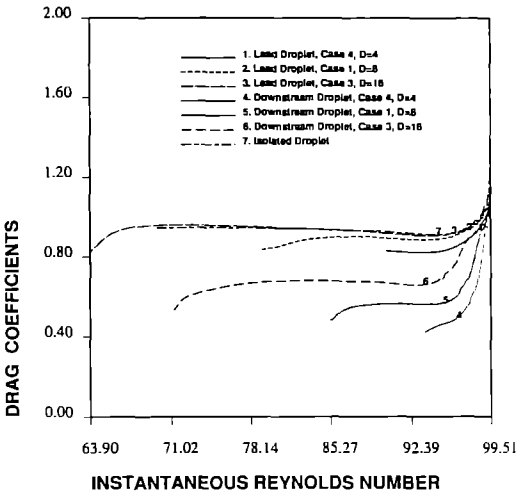

FIG. 11. Time variation of drag coefficients for the lead droplet and the downstream droplet for the cases of different initial droplet spacings.

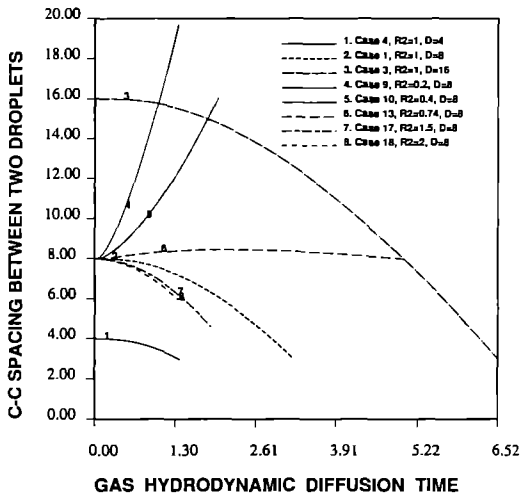

FIG. 10. Time variation of droplet spacing for the cases of different initial droplet spacings and for the cases of different initial droplet size ratios.

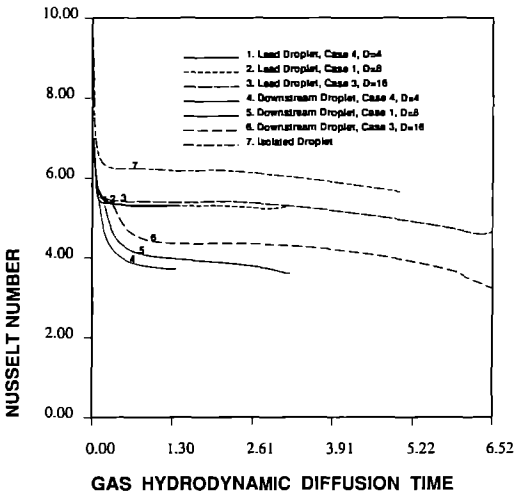

FIG. 12. Time variation of Nusselt numbers for the lead droplet and the downstream droplet for the cases of different initial droplet spacings.

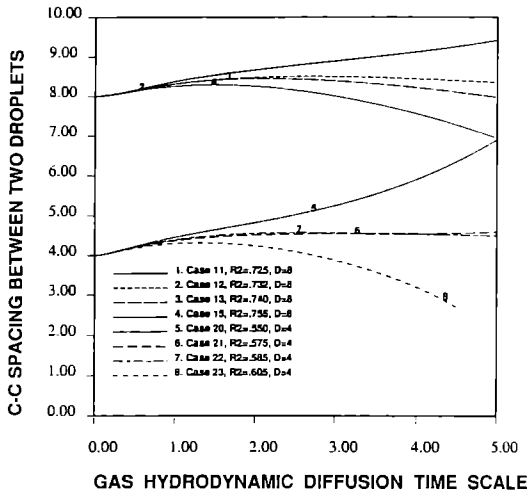

FIG. 13. Determination of the critical droplet size ratio for initial droplet spacing = 8, and for initial droplet spacing = 4.

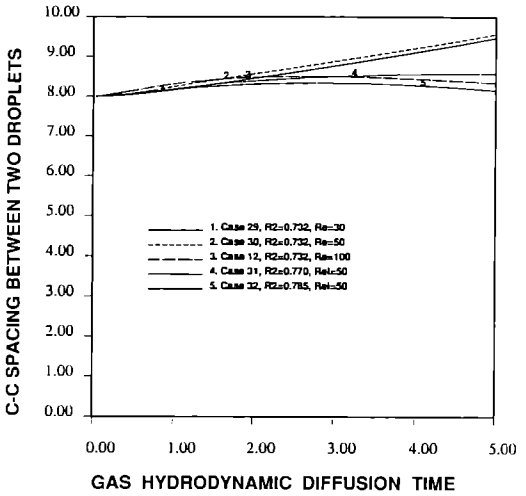

FIG. 15. Change droplet-motion pattern by changing initial Reynolds number when R_2/R_1 is close to the critical size ratio.

ible. The critical droplet size ratio for $D = 4$ is smaller than the ratio for $D = 8$ (0.585 vs 0.732), since the difference in drag coefficients of the two droplets becomes larger for smaller initial spacing. Since the constant-property calculation largely overestimates the drag coefficient more for the lead droplet than for the downstream droplet, it actually underestimates the critical droplet size ratio.

Figure 14 displays the drag coefficients of the two droplets for the cases of $R_2 \leqslant 1$. The drag coefficients of the lead droplets for the cases of smaller downstream droplets are all collapsed together. At this initial spacing, the lead droplet receives little influence from the downstream droplet. Also, the drag coefficients of the separating downstream droplets tend to increase with the reduction in Reynolds number; this is a typical characteristic of an isolated droplet.

Figure 15 indicates that by decreasing the initial Reynolds number for the case with droplet size ratio at the critical point, the droplet-motion pattern can be changed from collision to separation. The critical size ratio increases to 0.77 as the initial Reynolds number reduces to 50 for initial spacing = 8. From the results shown above, the determination of droplet separation or collision is dependent on the combined influence of the initial spacing and Reynolds number as well as the droplet size ratio.

The influence of the initial Reynolds number for the case of droplet collision is shown in Fig. 16. An increase in initial Reynolds number increases the approach speed. At low Reynolds number ($\leqslant 10$) flow, the convection effect is very small for both droplets such that the drag coefficients for the two droplets are almost the same. The spacing changes very slowly.

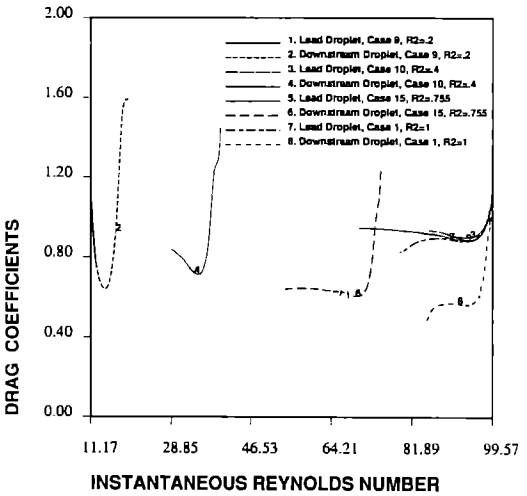

FIG. 14. Time variation of drag coefficients for the lead droplet and the downstream droplet for the cases of different initial droplet size ratios.

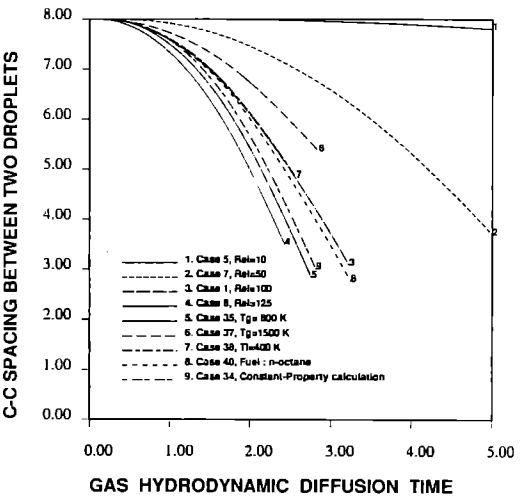

FIG. 16. Time variation of droplet spacings for the cases of different initial Reynolds numbers, different initial droplet temperatures, initial ambient temperatures, and fuel types.

The heat transfer number has significant influence in the computation of drag force, as well as heat and mass fluxes. The transient variation of droplet spacing is expected to be very dependent on the above effect. For high 'effective' heat transfer number cases, which correspond to the cases with high ambient temperature, high initial droplet temperature, or volatile fuel, the drag coefficients and transport rates are largely reduced to surface blowing. The rate of variation of droplet spacing is usually smaller than that of the low 'effective' transfer-number cases.

Correlations for drag coefficients and Nusselt and Sherwood numbers

The correlations for an isolated droplet very early in its lifetime, where the droplet possesses a low value of transfer number, are approximated by the following expressions from our previous study [19]

$$C_{D_\infty} = 24.432 Re_m^{-0.721}(1+B_{H,film})^{-0.27}$$

$$Nu_{film_\infty} = 1.275 Re_m^{0.438}\, Pr_{film}^{0.619}(1+B_{H,film})^{-0.678}$$

$$Sh_{film_\infty} = 1.224 Re_m^{0.385}\, Sc_{film}^{0.492}(1+B_{M,film})^{-0.568}$$

where $0 \leqslant B_{H,film} \leqslant 6$; $0 \leqslant B_{M,film} \leqslant 4.6$; $25 \leqslant Re_m \leqslant 200$.

These correlations are modified due to the proximity of other droplets. Since the droplet interaction effects are associated with the combined influences of the gas-phase convection, surface blowing and transient heating, and the relative motion between the droplets, the transfer coefficients depend upon instantaneous Reynolds and transfer numbers as well as the geometric factors related to the droplet motion. The present study has created a numerical database which covers a wide range of Reynolds and transfer numbers, size ratios and initial spacings. A linear regression model has been employed to yield the following correlations which fit reasonably accurately more than 3000 data points with different combinations of parameters.

For the lead droplet:

$$\frac{C_{D_1}}{C_{D_\infty}} = 0.877 Re_m^{-0.003} \times (1+B_{H,film})^{-0.040} D^{0.048}\left(\frac{R_2}{R_1}\right)^{-0.098}$$

$$\frac{Nu_{film_1}}{Nu_{film_\infty}} = 1.245 Re_m^{-0.073}\, Pr_{film}^{0.150} \times (1+B_{H,film})^{-0.122} D^{0.013}\left(\frac{R_2}{R_1}\right)^{-0.056}$$

$$\frac{Sh_{film_1}}{Sh_{film_\infty}} = 0.367 Re_m^{0.048}\, Sc_{film}^{0.730} \times (1+B_{M,film})^{0.709} D^{0.057}\left(\frac{R_2}{R_1}\right)^{-0.018}$$

where $0 \leqslant B_{H,film} \leqslant 1.06$; $0 \leqslant B_{M,film} \leqslant 1.29$; $11 \leqslant Re_m \leqslant 160$; $0.68 \leqslant Pr_{film} \leqslant 0.91$; $1.47 \leqslant Sc_{film} \leqslant 2.50$; $2.5 \leqslant D \leqslant 32$; $0.17 \leqslant R_2/R_1 \leqslant 2.0$.

For the downstream droplet:

$$\frac{C_{D_2}}{C_{D_\infty}} = 0.549 Re_m^{-0.098}(1+B_{H,film})^{0.132} D^{0.275}\left(\frac{R_2}{R_1}\right)^{0.521}$$

$$\frac{Nu_{film_2}}{Nu_{film_\infty}} = 0.528 Re_m^{-0.146}\, Pr_{film}^{-0.768} \times (1+B_{H,film})^{0.356} D^{0.262}\left(\frac{R_2}{R_1}\right)^{0.147}$$

$$\frac{Sh_{film_2}}{Sh_{film_\infty}} = 0.974 Re_m^{0.127}\, Sc_{film}^{-0.318} \times (1+B_{M,film})^{-0.363} D^{-0.064}\left(\frac{R_2}{R_1}\right)^{0.857}$$

where $0 \leqslant B_{H,film} \leqslant 2.52$; $0 \leqslant B_{M,film} \leqslant 1.27$; $11 \leqslant Re_m \leqslant 254$; $0.68 \leqslant Pr_{film} \leqslant 0.91$; $1.48 \leqslant Sc_{film} \leqslant 2.44$.

The Reynolds, Prandtl, Schmidt, and transfer numbers in the above two correlations pertain to the particular droplet described by the correlation.

The computation is stopped when the droplet spacing is reduced below 2.6 or whenever the downstream droplet approaches the outer computational boundary, since the grid generation routine can generate overskewed grid system under these conditions. Often the computation terminated at a very early stage of the droplet lifetime during which most of heat flux to the droplet surface would be transferred to the interior of the droplet. The effective transfer number

$$B_H = C'_{pg,film}(T'_\infty - T'_s)\left(1 - \frac{Q'_l}{Q'_g}\right)\Big/ L'_s$$

is quite low due to the high value for droplet heating ($(Q'_l/Q'_g) \approx 0.95$). For most cases, the downstream droplet was taken to be smaller than the lead droplet. The heat transfer to the downstream droplet is sufficient to complete the droplet heating so that the effective transfer number can reach a higher value. The comparisons of numerical solutions and correlations are given in Figs. 7–9. The numerical correlations indicate that the dependencies upon modified Reynolds and transfer numbers, Prandtl and Schmidt numbers are remarkable for the correlations of both droplets. However, the geometric parameters, while having significant influence on the downstream-droplet correlation, only play minor roles in the correlations of the lead droplet.

CONCLUSIONS

The present research on the interaction between two vaporizing droplets moving in tandem has improved our basic understanding and computational data base. The following conclusions have been drawn.

Due to the influence of recirculating flow from the lead droplet, the downstream droplet receives considerably less convection and hence less shear stress and less internal circulation. The drag coefficient of the lead droplet tends to be similar to that of an isolated droplet until the droplets are separated by less than 6 diameters. The drag coefficient of the downstream droplet is significantly lower than that of the lead droplet. A similar trend for the Nusselt and Sherwood numbers is also observed. The dominant type of internal heating of the downstream droplet switches to conduction as the two droplets become sufficiently close that the downstream droplet reaches the near wake of the lead droplet.

Droplet trajectories are also analyzed for a wide range of initial Reynolds number, initial droplet spacing, initial droplet size ratio, and transfer number. Results indicated that droplet spacing could increase or decrease in time depending upon various factors. Separation becomes more likely as the downstream droplet becomes smaller relative to the lead droplet. For each initial droplet spacing, there exists a critical droplet-size ratio below which the droplet collision becomes unlikely. For decreasing initial spacing, the drag difference increases and the critical size ratio decreases. The critical size ratio increases as the initial Reynolds number decreases. An increase in initial Reynolds number serves to increase the approaching speed. The results from constant property computations overestimate the approaching (or separating) speed of the downstream droplet. For the cases with high transfer number, the rate of variation of droplet spacing is reduced. The correlations for the transfer coefficients of both droplets have been obtained and can be applied in the overall spray computations.

Acknowledgements—This work has been supported by the Air Force Office of Scientific Research under grant No. 86-0016-D with Dr Julian Tishkoff acting as the program manager. The authors thank Dr M. S. Raju for assistance in comparing the constant-property code. The support of the Pittsburgh Supercomputing Center under an Advanced Computing Resources Grant of the National Science Foundation as well as the Office of Academic Computing at UCI are greatly appreciated.

REFERENCES

1. J. Happel and H. Brenner, *Low Reynolds Number Hydrodynamics*, Chap. 6. Prentice-Hall, Englewood Cliffs, NJ (1965).
2. G. K. Batchelor and J. T. Green, The hydrodynamic interaction of two small freely-moving spheres in a linear flow field, *J. Fluid Mech.* **56**, 375–400 (1972).
3. D. J. Jeffrey and Y. Onishi, Calculation of the resistance and mobility functions for two unequal rigid spheres in low Reynolds number flow, *J. Fluid Mech.* **139**, 261–290 (1984).
4. R. Tal (Thau) and W. A. Sirignano, Cylindrical cell model for the hydrodynamics of particle assemblages at intermediate Reynolds numbers, *A.I.Ch.E. Jl* **28**, 233–236 (1984).
5. R. Tal (Thau), D. N. Lee and W. A. Sirignano, Heat and momentum transfer around a pair of spheres in viscous flow, *Int. J. Heat Mass Transfer* **27**, 1953–1962 (1984).
6. E. M. Twardus and T. A. Brzustowski, The interaction between two burning fuel droplets, *Archiwum Processor Spalania* **8**, 347–358 (1977).
7. M. Labowsky, A formalism for calculating the evaporation rates of rapidly evaporating interacting particles, *Combust. Sci. Technol.* **18**, 145 (1977).
8. M. Labowsky, Calculating of burning rates of interacting fuel droplets, *Combust. Sci. Technol.* **22**, 217–226 (1980).
9. A. Umemura, A. Ogawa and N. Oshiwa, Analysis of the interaction between two burning droplets, *Combust. Flame* **41**, 45–55 (1981).
10. A. Umemura, A. Ogawa and N. Oshiwa, Analysis of the interaction between two burning droplets with different sizes, *Combust. Flame* **43**, 111–119 (1981).
11. T. Y. Xiong, C. K. Law and K. Miyasaka, Interactive vaporization and combustion of binary droplet system, *Proc. 20th Int. Symp. on Combustion*, Combustion Inst., Pittsburgh, PA, pp. 1781–1787 (1985).
12. W. A. Sirignano, Fuel droplet vaporization and spray combustion theory, *Prog. Energy Combust. Sci.* **9**, 291–322 (1983).
13. Koichi Asano, Izumi Taniguchi and Takahiro Kawahara, Numerical and experimental approaches to simultaneous evaporation of two adjacent volatile drops, *Proc. 4th Int. Conf. on Liquid Atomization and Spray Systems*, pp. 411–418 (1988).
14. G. Patnaik, *A numerical solution of droplet vaporization with convection*, Ph.D. Dissertation, Carnegie-Mellon University, Department of Mechanical Engineering (1986).
15. G. Patnaik, W. A. Sirignano, H. A. Dwyer and B. R. Sanders, A numerical technique for the solution of a vaporizing fuel droplet, *Progress in Astronautics and* Aeronautics **105**, pp. 253–266. AIAA Inc., Washington, DC (1986).
16. M. S. Raju and W. A. Sirignano, Unsteady Navier–Stokes solution for two vaporizing droplets, *AIAA Aerospace Sciences Meeting*, Paper 87-0300 (1987).
17. M. S. Raju and W. A. Sirignano, Interaction between two vaporizing droplets in an intermediate-Reynolds-number flow, *Physics Fluids A* **2**(10), 1780–1796 (1990).
18. J. F. Thompson, F. C. Thames and C. W. Mastin, Boundary-fitted curvilinear coordinate system for solution of partial differential equations on fields containing any number of arbitrary two-dimensional bodies, *NASA CR-2729* (1976).
19. C. H. Chiang, M. S. Raju and W. A. Sirignano, Numerical analysis of convecting, vaporizing fuel droplet with variable properties, *Int. J. Heat Mass Transfer* **35**, 1307–1324 (1992).
20. J. F. Thompson, Z. U. A. Warsi and C. W. Mastin, *Numerical Grid Generation: Foundations and Applications*, Chap. 3. North-Holland, New York (1985).
21. S. Temkin and G. Z. Ecker, Droplet pair interactions in a shock-wave flow field, *J. Fluid Mech.* **202**, 467–497 (1989).
22. R. J. Haywood, N. Nafziger and M. Renksizbulut, A detailed examination of gas and liquid phase transient processes in convective droplet evaporation, *J. Heat Transfer* **111**, 495–502 (1989).